# AN INVESTIGATION OF THE FATIGUE STRENGTH OF MULTIPLE CELLULAR STRUCTURES FABRICATED BY ELECTRON BEAM POWDER BED FUSION ADDITIVE MANUFACTURING PROCESS

Abigail Orange[*], Yan Wu[†], Li Yang[†]

*Department of Mechanical Engineering, University of Louisville, Louisville, KY 40292
†Department of Industrial Engineering, University of Louisville, Louisville, KY 40292

## Abstract

In this study multiple cellular structures, including the re-entrant auxetic, the octet-truss, and the BCC lattice, were evaluated for their relative performance of fatigue strength under compression-compression cyclic loading. Various design variations with different dimensions were fabricated via electron beam powder bed fusion (EB-PBF) additive manufacturing (AM) process and experimentally tested. Initial S-N based fatigue strength characterization with the BCC lattice shows significantly decreased fatigue strength of the cellular parts compared to the solid samples. Cross-design comparison were consequently carried out using constant maximum stress ratio level. The results indicate that the fatigue characteristics of the EB-PBF cellular structures are not only dependent on their topology types but also their geometry dimensions.

## Introduction

Direct fabrication of metallic cellular structures using additive manufacturing (AM) has been extensively demonstrated in various research works and case studies [1-6]. It is widely expected that these structures have vast potentials in a broad range of applications by providing outstanding mechanical properties per unit mass [7-9]. On the other hand, for many applications the reliability of the components over the entire service life is of critical importance, which imposes significant challenges to the design and manufacturing of the lightweight structures due to their generally reduced design redundancy. For many AM-fabricated structures, this issue could be further aggravated by the tendency of developing both surface and internal defects during the fabrication processes [4, 6, 10, 11]. For example, for powder bed fusion (PBF) AM processes, due to the use of powder feedstock with random particle size distributions, the resulting parts generally exhibit certain levels of surface roughness and internal porosities, which can become detrimental to various performance characteristics of the fabricated cellular structures such as the fatigue endurance.

In previous literature, the fatigue properties of the cellular structures fabricated by the PBF-AM processes was briefly investigated [12-15]. The results generally suggest that the PBF-AM cellular structures exhibit significantly lower fatigue strength compared to both the traditional foam structures and the solid PBF-AM parts of the same materials [16-19]. For the solid PBF-AM parts, the two primary source of defects that contribute to the reduced fatigue strength are the internal pores/defects and the surface roughness [19, 20]. On the other hand, while it was suggested that fatigue strength comparable to that of traditional materials can be achieved for PBF-AM structures via adequate surface finish treatment such as machining [19], such treatment is generally infeasible for the cellular structures that exhibit complex geometries, which result in the high possibility for crack initiation from surfaces for these structures [13-15]. In addition to the aforementioned two

sources of defects, the PBF-AM cellular structures also exhibit intrinsic quality variability that could introduce further performance fluctuation [12].

The reported fatigue strength of the Ti6Al4V cellular structures fabricated by electron beam melting AM (EBM-AM) is generally in the range of $0.15-0.25\sigma_{YS}$ for the $10^6$ cycle life criteria, where $\sigma_{YS}$ is the yield strength of the solid material [12-14]. Multiple cellular structure designs were used for the experimental studies, including the dodecahedron [12], the BCC lattice [13], and the hexagonal/diamond lattice [14] as shown in Fig.1, and although the fatigue strength of these structures show consistently low values, it was also suggested that the geometry factor might potentially play a role in the fatigue performance of the structures [12]. As there currently exist very little knowledge in identifying the potential impact of geometry designs of cellular structures on their fatigue performance, the objective of this work is to provide preliminary experimental insights into this area.



| a. Dodecahedron [12] | b. BCC lattice [13] | c. Hexagonal/diamond lattice [14] |
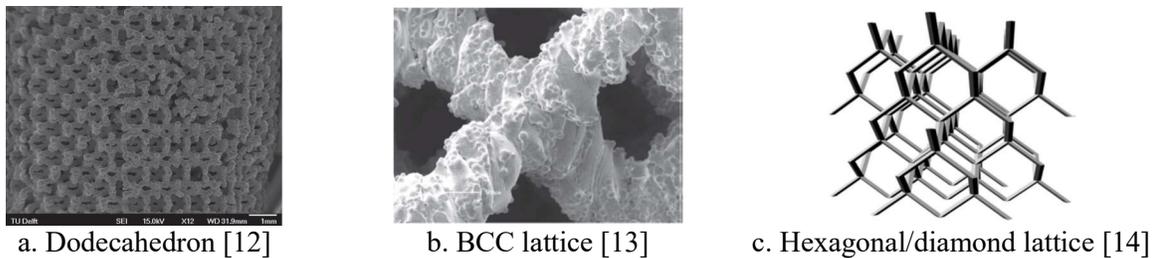
Fig.1 Cellular structure designs previously evaluated for fatigue performance

### Sample design, fabrication and testing procedure

There exist infinite possibilities of geometry designs for the cellular structures, and it is infeasible to establish a comprehensive experimental database for the cellular "materials". Therefore in the current study multiple cellular designs with distinct design mechanisms were investigated in the attempt to improve the representativeness of the results. Fig.2 shows the four designs used in the current study, which are octet-truss, BCC lattice, octahedral and re-entrant auxetic structures. The octet-truss is a stretch-dominated design with high degrees of structural symmetry, the BCC lattice is a bending-dominated design also with high degrees of structural symmetry, the octahedral lattice is a stretch-dominated design with lower degrees of symmetry, and lastly the re-entrant auxetic structure is a bending-dominated design with negative Poisson's ratio [21]. The geometrical design variables for each types of unit cell designs are also shown in Fig.2, and for the current study the setting of these parameters are listed in Table 1. One of the basic criteria used in the design of the unit cell geometrical parameters is the relative density (RD). For all four types of unit cell designs, two levels of RD, ~0.1 and ~0.2, were introduced into the designs by varying geometry parameters. In addition, for the unit cell structures that exhibit low degrees of symmetry (BCC and re-entrant auxetic), additional design variations were introduced to evaluate the effects of unit cell height to lateral width aspect ratios at the same level of RD (Aux-1 vs. Aux-3, BCC-1 vs. BCC-3). The RD values were calculated from the CAD models with each of the unit cell designs. The patterns used for the RD calculations were 4x4x4 patterns for all the designs, which were also used for the fabrication of the actual samples. It is noted that even though the pattern size of the cellular structures are relatively small, from the previous studies it can be argued that the boundary effect

is stabilized by the adoption of the same numbers of repetition (4) in all principal directions of the designs [22].

| Design | H (mm) | L/L$_1$ (mm) | θ (deg)/L$_2$ (mm) | t (mm) | RD |
|---|---|---|---|---|---|
| Aux-1 | 5 | 3.5 | 70 | 1 | 0.205 |
| Aux-2 | 7 | 5.5 | 70 | 1 | 0.104 |
| Aux-3 | 7 | 3.5 | 60 | 1 | 0.193 |
| Octet-1 | | 6 | | 1 | 0.198 |
| Octet-2 | | 8.8 | | 1 | 0.101 |
| BCC-1 | 2.7 | 5.4 | 5.4 | 1 | 0.192 |
| BCC-2 | 3.5 | 7 | 7 | 1 | 0.105 |
| BCC-3 | 2 | 6.2 | 6.2 | 1 | 0.197 |
| Oct-1 | | 5.4 | | 1 | 0.187 |
| Oct-2 | | 7.6 | | 1 | 0.104 |

Table 1 Design parameters for the cellular structures



a. Octet-truss          b. BCC          c. Octahedral          d. Re-entrant auxetic
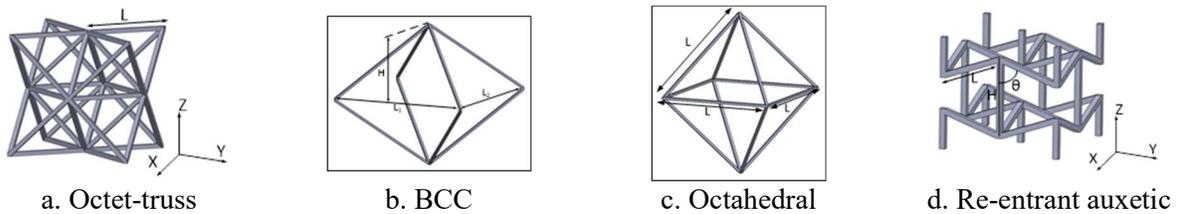
Fig.2 Cellular unit cell designs investigated

All the samples were fabricated by an Arcam electron beam melting (EBM) S400 system using Ti6Al4V-ELI as material. Fig.3 shows some of the fabricated samples. As the study mainly focused on the investigation of geometry effects, no attempt was made to specifically characterize the powder feedstock characteristics or optimize the process parameters. The default canned process parameters for the cellular structures (Ti6Al4V-Net) was adopted for the setting. 5-10 samples of each design variation were fabricated. The overall dimensions and weights of the samples were measured using a caliper in order to calculate the actual RD of each samples. Table 2 shows the measurement and calculation results for the samples. The densities of the actual samples of all designs were significantly lower than the designed values while exhibiting high consistency. In addition, for each type of design, one arbitrary sample was selected for strut dimension measurement using digital optical microscope. The maximum inscribed diameter $D_i$ as shown in Fig.4 was taken as the diameter of the struts from the digital images, and the results are shown in Table 3 (results from 3 arbitrarily struts of an arbitrarily sample). Some of the measurements were incorrectly taken by the operator and thus became unavailable. The auxetic and octahedral samples exhibit relatively significant strut dimensional deviations from the nominal designs (1mm), which does not agree well with the observations from similar studies in previous literature [23, 24]. On the other hand, such dimensional deviations do not fully account for the reduced densities as shown in the CAD relative density values in Table 2 calculated from the updated models using measured strut dimensions. Therefore, it was speculated that the struts of all the cellular structures exhibit additional internal porosities, possibly due to the beam quality issues such as calibration or astigmatic errors.

Fig.3 Some fabricated Ti6Al4V samples

| Design | CAD model | | | Actual sample | | | RD | CAD RD |
|---|---|---|---|---|---|---|---|---|
| | $D_1$ (mm) | $D_2$ (mm) | $D_3$ (mm) | $D_1$ (mm) | $D_2$ (mm) | $D_3$ (mm) | | |
| Aux-1 | 27.31 | 27.31 | 30.42 | 27.46±0.19 | 27.65±0.27 | 30.22±0.06 | 0.154±0.000 | 0.169 |
| Aux-2 | 42.35 | 42.35 | 40.95 | 42.50±0.12 | 42.52±0.12 | 40.65±0.31 | 0.072±0.001 | 0.083 |
| Aux-3 | 25.25 | 25.25 | 42.00 | 25.37±0.11 | 25.37±0.09 | 41.59±0.29 | 0.139±0.001 | 0.144 |
| Octet-1 | 34.94 | 34.94 | 34.94 | 35.17±0.23 | 35.13±0.17 | 34.65±0.22 | 0.141±0.004 | - |
| Octet-2 | 50.78 | 50.78 | 50.78 | 50.81±0.08 | 50.88±0.02 | 50.29±0.05 | 0.072±0.003 | - |
| BCC-1 | 21.60 | 21.60 | 22.12 | 21.65±0.09 | 21.72±0.13 | 21.70±0.22 | 0.138±0.007 | 0.182 |
| BCC-2 | 28.00 | 28.00 | 36.44 | 28.12±0.27 | 28.06±0.14 | 35.90±0.30 | 0.075±0.003 | 0.114 |
| BCC-3 | 24.80 | 24.80 | 16.64 | 24.35±0.56 | 24.94±0.12 | 16.55±0.16 | 0.146±0.004 | 0.168 |
| Oct-1 | 23.40 | 23.40 | 32.09 | 23.49±0.08 | 23.49±0.11 | 31.75±0.11 | 0.128±0.005 | 0.157 |
| Oct-2 | 31.40 | 31.40 | 43.41 | 31.42±0.09 | 31.46±0.07 | 42.78±0.09 | 0.074±0.002 | - |

Table 2 Dimensional measurements with fabricated Ti6Al4V samples
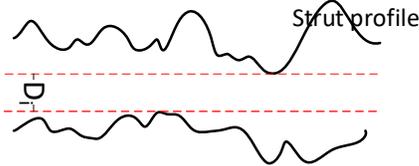

Fig.4 Inscribed strut diameter measurement

| Design | Strut type | Actual sizes (mm) |
|---|---|---|
| Aux-1 | Vertical | 1.04±0.03 |
| | Re-entrant | 0.86±0.10 |
| Aux-2 | Vertical | 0.75±0.04 |
| | Re-entrant | 0.98±0.02 |
| Aux-3 | Vertical | 0.77±0.00 |
| | Re-entrant | 0.95±0.02 |
| BCC-1 | | 0.97±0.02 |
| BCC-2 | | 0.97±0.05 |
| BCC-3 | | 0.91±0.02 |
| Oct-1 | Horizontal | 1.05±0.05 |
| | Vertical | 0.86±0.05 |

Table 3 Strut diameter

One arbitrarily selected sample of each design were subjected to quasi-static compressive testing under an Intron 5569A with a loading rate of 1mm/min. The sample size of one was largely due to the limitation of resource availability but was also considered to be acceptable due to the observed consistency with the qualities of the parts as well as the conclusions from previous literatures with Ti6Al4V fabricated by EB-PBF [23, 25, 26]. The ultimate strength ($\sigma_m$) of each types of cellular structures were taken as the references for the configuration of the compression-compression fatigue testing. The use of ultimate strength was note expected to affect the interpretation of the fatigue strength as the Ti6Al4V struts fabricated by EB-PBF generally exhibit little yield and was therefore considered "brittle" for the purpose of initial failure strength estimation [23].

For the fatigue testing, firstly the compression-compression cyclic testing with varying maximum stress level $\sigma_{max}/\sigma_m$ = 0.1, 0.2, 0.4 and 0.5 and stress ratio R=$\sigma_{peak}/\sigma_{valley}$=0.1 was carried out with the BCC-1 samples, where $\sigma_{max}$ is the maximum stress levels applied to the sample, and $\sigma_{peak}$ and $\sigma_{valley}$ are the maximum and minimum compressive stress levels within a single compression-

compression cycle, respectively. The purpose of such study was to establish a reference S-N curve in attempt to determine a proper value of $\sigma_{max}/\sigma_m$ for all the designs so that sufficiently slow crack growth could be ensured while limiting the total testing time. The BCC-1 structure was selected for the S-N curve study as most samples of this design were fabricated. Following the S-N curve study, a fixed level $\sigma_{max}/\sigma_m$ value was selected, and samples of the other designs were subjected to the compressive-compressive cyclic testing with the same R=0.1 configuration. All the fatigue testing was carried out on an Instron Electroplus E10000 system with samples compressed between two steel platens. The waveform for the cyclic loading was sinusoidal, and all the testing was executed under the force-controlled mode at 50Hz cycle frequency.

## Results and analysis

The static compressive testing results for each type of the structures are listed in Table 4. In order to estimate the potential impact of the strut dimension deviations, additional finite element simulations with each designs were carried out using the measured strut dimensions results for each corresponding designs. The samples generally exhibit significantly lower strength compared to the CAD models even after the strut dimension compensation, which clearly indicates the existences of internal porosities. Although the density deviation issue was previously reported for EB-PBF cellular parts [26], many literature have shown that the EB-PBF process using Arcam systems is capable of producing generally high-quality cellular parts [5, 24, 25]. Therefore it is likely that the system used to fabricate the samples was not tuned to the optimal operation conditions. The S400 system used in this study utilizes a completely manual beam calibration protocol that heavily relies on the operator's level of expertise, which in combination with the nonlinear nature of the electrical optics systems, makes it more problematic for these older generation systems to maintain consistent qualities over elongated service period.

| Design | Maximum force (N) | Comp. strength (MPa) | FEA strength (MPa) | Diff. (%) |
|---|---|---|---|---|
| Aux-1 | 6417 | 8.30 | 9.52 | 12.8% |
| Aux-2 | 2990 | 1.66 | 1.70 | 2.3% |
| Aux-3 | 8812 | 13.66 | 10.91 | 25.2% |
| Octet-1 | 13467 | 14.08 | 10.06 | 40.0% |
| Octet-2 | 8022 | 3.05 | 4.08 | 25.2% |
| BCC-1 | 5366 | 11.37 | 10.95 | 3.8% |
| BCC-2 | 2812 | 3.40 | 4.36 | 22.1% |
| BCC-3 | 3925 | 6.56 | 7.31 | 10.2% |
| Oct-1 | 5209 | 9.27 | 21.48 | 56.84% |
| Oct-2 | 3337 | 3.38 | 14.67 | 77.0% |

Table 4 Quasi-static mechanical strength of the fabricated samples

The S-N curve for the BCC-1 design was obtained experimentally and shown in Fig.5. The dashed line with an arrow in Fig.5 indicates that the sample at 10% maximum stress level did not fail after 2 million cycles, and therefore was taken as the fatigue limit of this structure. The results appear to agree well with the previous studies with EB-PBF cellular structures [12-14]. However, since only one sample was tested at each maximum stress levels, this S-N curve was not intended to provide accurate information of the fatigue characteristics of the structures. Based on the results, the 20% maximum stress level was selected for the rest of the designs since at this level the BCC-1 structure appears to exhibit stable fatigue crack progression and that the duration of the cyclic testing was acceptable for the test schedule.
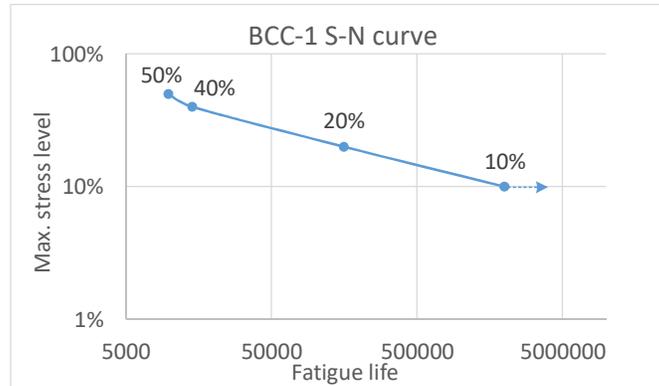
Fig.4 S-N curve of BCC-1 design based on single-sample testing

3-5 samples of each designs were subjected to the compressive-compressive cyclic loading per the setting previously described. Due to the "tune-in" process with the tester during the beginning of each test, the maximum and minimum loading levels of each cycle curing this period tend to be significantly smaller than the set values. Therefore the results from the first 100 cycles were subsequently discarded during the processing of the results. Fig.5 shows the cumulative strains of all different types of designs, which were obtained by calculating the progressive shortening/crushing of the samples using the initial strains as references. In general there exist significant differences among the cumulative strains of different types of designs as well as among the same type of structures. For the traditional foam cellular structures, there typically exist three stages of strain accumulation, namely the incubation stage, the steady state stage, and the accelerated collapse stage [27-29]. The incubation stage is driven by the formation of the crack initiations, which is then followed by the progressive crack propagation during the steady state stage. During the final stage, due to the widespread presence of cracks and fractured struts, the cellular structure exhibits catastrophic failure by forming crushing bands across the entire structures. For many the cellular structures evaluated in the current study, the incubation stages appear to be very short or near absent, which might correspond to two types of mechanisms. For structures that exhibit very short incubation stages such as Aux-3, BCC-1 and BCC-2 structures, the shortened crack initiation period might be attributed to the extensive existence of defects with the fabricated structures. On the other hand, for structures that exhibit absence of the initial incubation stage such as Aux-1, Aux-2, BCC-1, BCC-2, Oct-1 and Oct-2, there might exist specific sites or locations that predominantly determine the initiation and propagation of the cracks. The later mechanism was also observed from previous studies with the EB-PBF cellular structures [12, 13]. Compared to the typical behaviors of the stochastic cellular structures (e.g. foams), the stress and strain status of individual struts in the periodic cellular structures can be more readily determined, which is believed to be closely associated with the crack propagation characteristics observed from this study and could be potentially beneficial for applications where the fatigue failure of the structures needs to be designed. In comparison, the octet-truss structures exhibit the typical three-stage strain accumulation characteristics, which might be attributed by the relatively small stress gradients within the structures and consequently lack of dominant crack propagation patterns, as well as less sensitivity towards defects in individual struts. It is likely that further investigations will be needed to verify such speculation.

a. Aux-1　　　　　　b. Aux-2　　　　　　c. Aux-3

d. Octet-1　　　　　　　　　e. Octet-2

f. BCC-1　　　　　　g. BCC-2　　　　　　h. BCC-3

i. Oct-1　　　　　　　　　j. Oct-2
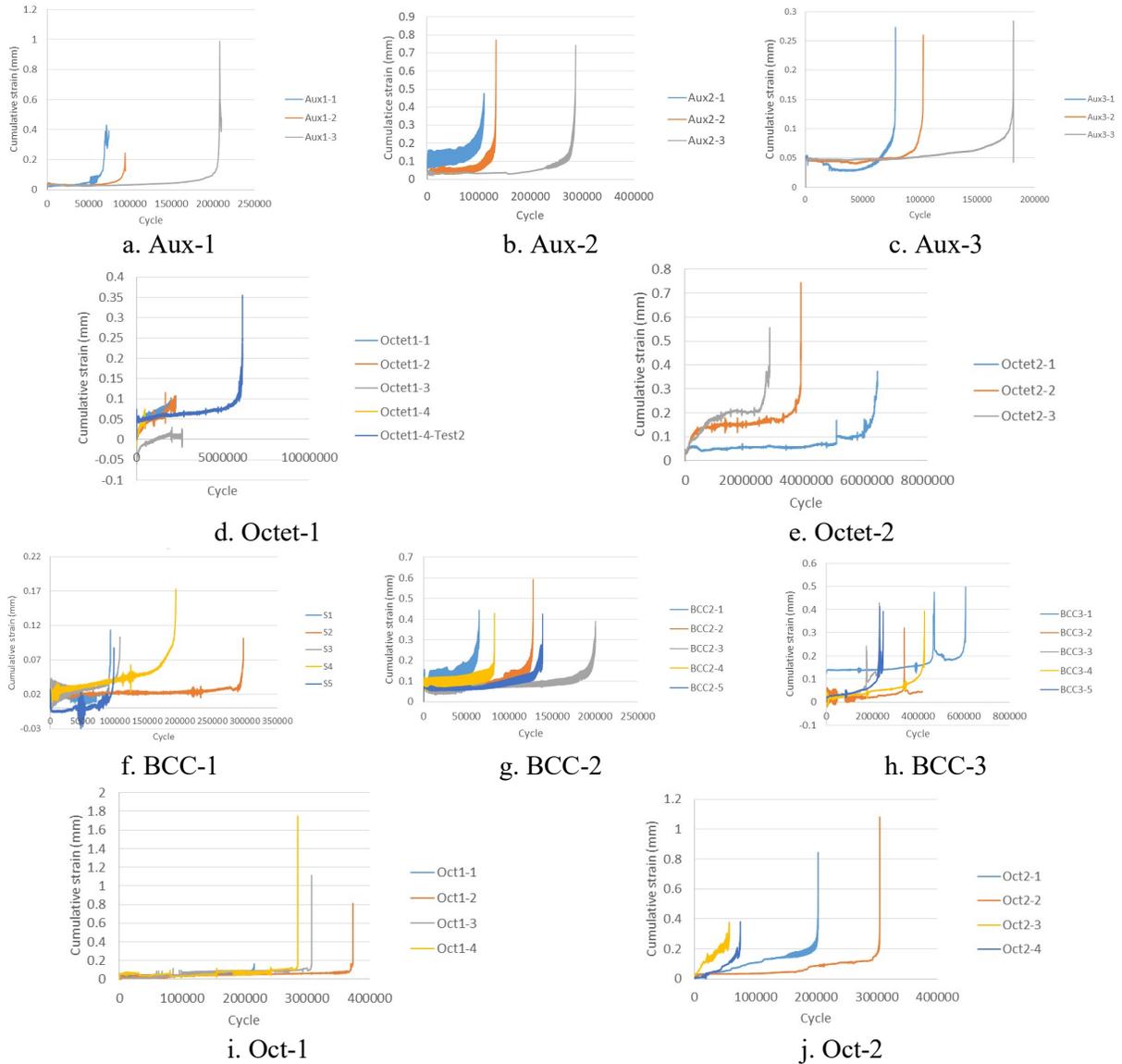
Fig.5 Cumulative strain under cyclic loading for each type of designs

Towards the end of the cyclic testing, all the designs exhibited very high strain accumulation rate that cause rapid crushing of the structures within a few cycles. For octahedral structures catastrophic failure occurs within a single loading cycle. This is in agreement to the formation of distinct "layerwise" crush patterns or shear patterns, which is associated with the well-defined geometries of these structures and was previously observed with the cellular structures fabricated via PBF-AM [23].

a. Aux-1      b. Aux-2      c. Aux-3

d. Octet-1      e. Octet-2

f. BCC-1      g. BCC-2      h. BCC-3

i. Oct-1      j. Oct-2
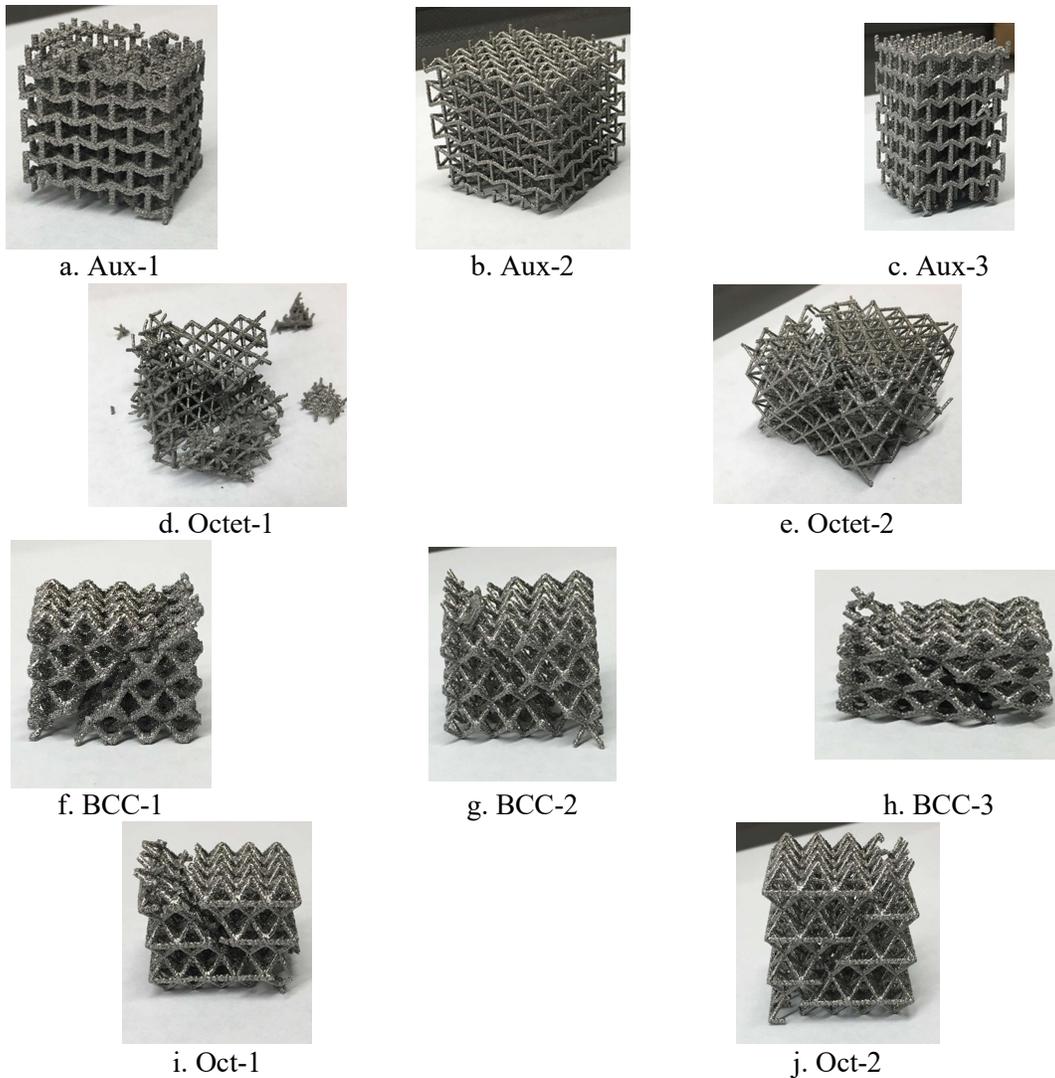
Fig.6 Typical samples of each designs after the fatigue testing

Fig.6 shows the typical samples of each designs at the end of the testing after the rapid strain accumulation stages. All the designs with positive Poisson's ratios exhibit the diagonal "shear" fracture patterns, which were formed during the final catastrophic failure stages. Among these, the octet-truss structures appear to have sustained more extensive damages, with more macroscopic fracture bands clearly discernable throughout the samples. On the other hand, for the auxetic structures no apparent fracture planes were discernable, and upon closer check large numbers of fractured debris were found to be not completely detached from the structures. From previous studies with this structure it was concluded that the auxetic structures generally exhibit superior energy dissipation and reduced stress concentration upon loading, which might have contributed to the unique fatigue fracture characteristics of these structures.

Based on the strain accumulation characteristics of all the designs, a cumulative strain/displacement of 0.2mm was selected as the failure criteria in order to establish the estimations of fatigue strength. Fig.7 shows the fatigue life of each types of cellular designs. The octet-truss structures clearly exhibit significantly higher fatigue life, with both design variations

failing at over 3 million cycles. Fig.8 further maps the fatigue lives of different cellular designs against their relative densities. The results show that the relative densities evaluated in the current study do not have significant effect on the fatigue performance of any of the cellular designs. Considering that relatively low levels of relative densities (<0.25) were investigated in the study, it is expected that the stress-strain characteristics of individual struts within these structures are reasonably linear during the cyclic testing. Also, the identical cross sectional dimension design (1mm) of struts for all the designs also facilitated the consistency of the fabrication qualities, which contributed to the relative density-independent behaviors. As for the effect of the design mechanisms on the fatigue performance of the structures, the effects of Poisson's ratio or structural symmetry appear to be insignificant, whereas the combination of deformation mode and structural symmetry (i.e. octet-truss versus octahedral) show significant effects. Considering that in the octet-truss structures strut bending contributes much less to overall deformation compared to the octahedral designs, it was speculated that such deformation mode is responsible for the superior fatigue performance of the octet-truss designs. From Fig.6 it also appears that the energy dissipation of the octet-truss designs is more extensive throughout the structures.
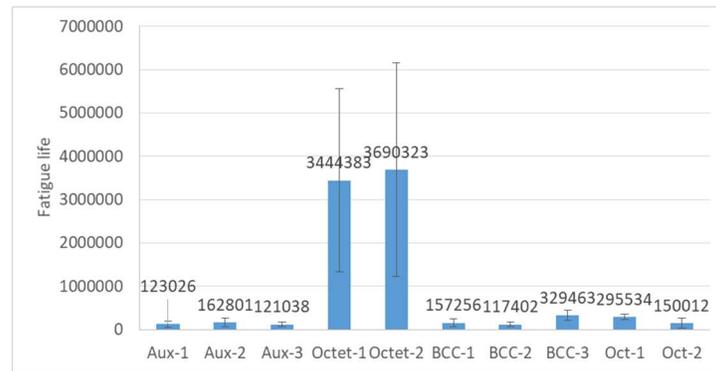


Fig.7 Fatigue life of each types of cellular designs
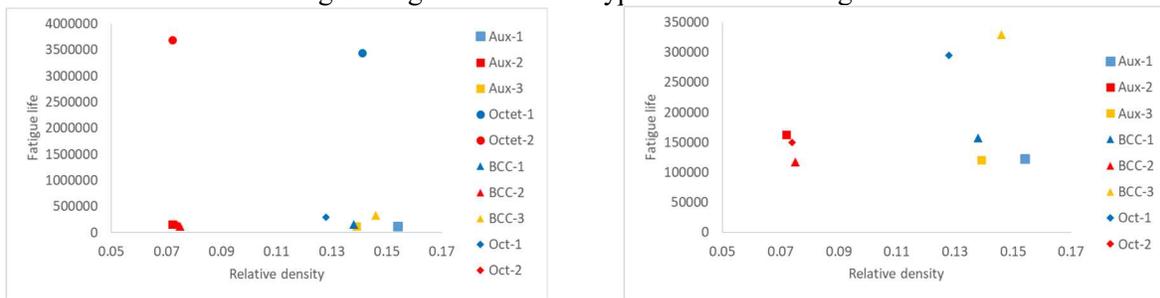


a. All structures            b. Octet-truss excluded

Fig.8 Relative density-fatigue life mapping of different designs

## Conclusions

In this work experimental studies were carried out to evaluate the potential effect of geometry designs on the fatigue performance of cellular structures fabricated via EB-PBF process. Due to the extensive presence of defects with the fabricated samples partly attributed to the calibration issue with the EB-PBF system used in the study, both the static and fatigue properties of the cellular structures were expected to be affected. On the other hand, the comparison among different designs indicates that the EB-PBF cellular structures exhibit distinct strain accumulation during the cyclic compression-compression loading. Most structures exhibit very short incubation stage during

which the initial cracks form, which likely attributed to the extensive defects that are present in the structures. After the steady strain accumulation stage, all the structures exhibit rather catastrophic failure during the final accelerated strain accumulation stage, which might be attributed to the less stochastic fracture pattern resulted from the pre-determined geometry designs. From the results, the cellular designs that exhibit significant strut bending deformation mode also exhibit lower fatigue performance in comparison to the designs that exhibit predominantly strut stretch/compression deformation mode (octet-truss). Structures with negative Poisson's ratios exhibit less-defined fracture patterns likely due to the ability of the structures for more homogenous stress distribution. On the other hand, the Poisson's ratio and relative density do not appear to play significant roles in the fatigue lives of different designs. As a result, octet-truss designs exhibit significantly higher fatigue life compared to the other structures. All the cellular structure designs exhibit low fatigue strength that is in agreement with previous studies, although it was also revealed that structural designs could play potentially important roles in their fatigue performance.

## Reference
[1] M. Leary, M. Mazur, J. Elambasseril, M. McMillan, T. Chirent, Y. Sun, M. Qian, M. Easton, M. Brandt. Selective laser melting (SLM) of AlSi12Mg lattice structures. Materials and Design. 98(2016): 344-357.
[2] C. B. Williams, J. K. Cochran, D. W. Rosen. Additive manufacturing of metallic cellular materials via three-dimensional printing. International Journal of Advanced Manufacturing Technologies. 53(2011): 231-239.
[3] X. Y. Cheng, S. J. Li, L. E. Murr, Z. B. Zhang, Y. L. Hao, R. Yang, F. Medina, R. B. Wicker. Compression deformation behavior of Ti-6Al-4V alloy with cellular structures fabricated by electron beam melting. Journal of the Mechanical Behavior of Biomedical Materials. 16(2012): 153-162.
[4] R. Gumruk, R. A. W. Mines. Compressive behaviour of stainless steel micro-lattice structures. International Journal of Mechanical Sciences. 68(2013): 125-139.
[5] O. Cansizoglu, O. Harrysson, D. Cormier, H. West, T. Mahale. Properties of Ti-6Al-4V non-stochastic lattice structures fabricated via electron beam melting. Materials Science and Engineering A. 492(2008): 468-474.
[6] C. Yan, L. Hao, A. Hussein, D. Raymont. Evaluations of cellular lattice structures manufactured using selective laser melting. International Journal of Machine Tools and Manufacture. 62(2012): 32-38.
[7] L. J. Gibson, M. F. Ashby. Cellular Solids: Structure and Properties. 2nd Edn. Cambridge University Press, 1997.
[8] D. W. Rosen. Design for additive manufacturing: a method to explore unexplored regions of the design space. The Proceedings of the International Solid Freeform Fabrication (SFF) Symposium, Austin, TX, 2007.
[9] L. Yang, O. L. A. Harrysson, D. Cormier, H. West, S. Zhang, H. Gong, B. Stucker. Design for additively manufactured lightweight structure: a perspective. The Proceedings of the International Solid Freeform Fabrication (SFF) Symposium, Austin, TX, 2016.
[10] I. Maskery, N. T. Aboulkhair, A. O. Aremu, C. J. Tuck, I. A. Ashcroft, R. D. Wildman, R. J. M. Hague. A mechanical property evaluation of graded density Al-Si10-Mg lattice structures manufactured by selective laser melting. Materials Science and Engineering A. 670(2016): 264-274.

[11] E. Hernandez-Nava, C. J. Smith, F. Derguti, S. Tammas-Williams, F. Leonard, P. J. Withers, I. Todd, R. Goodall. The effect of defects on the mechanical response of Ti-6Al-4V cubic lattice structures fabricated by electron beam melting. Acta Materialia. 108(2016): 279-292.

[12] S. A. Yavari, R. Wauthle, J. van der Stok, A. C. Riemslag, M. Jassen, M. Mulier, J. P. Kruth, J. Schrooten, H. Weinans, A. A. Zadpoor. Fatigue behavior of porous biomaterials manufactured using selective laser melting. Materials Science and Engineering C. 33(2013): 4849-4858.

[13] S. J. Li, L. E. Murr, X. Y. Cheng, Z. B. Zhang, Y. L. Hao, R. Yang, F. Medina, R. B. Wicker. Compression fatigue behavior of Ti-6Al4V mesh arrays fabricated by electron beam melting. Acta Materialia. 60(2012): 793-802.

[14] N. W. Hrabe, P. Heinl, B. Flinn, C. Korner, R. K. Bordia. Compression-compression fatigue of selective electron beam melted cellular titanium (Ti-6Al-4V). Journal of Biomedical Materials Research B Applied Biomaterials. 99(2011), 2: 313-320.

[15] S. A. Khanoki, D. Pasini. Fatigue design of a mechanically biocompatible lattice for a proof-of-concept femoral stem. Journal of the Mechanical Behavior of Biomedical Materials. 22(2013): 65-83.

[16] B. Torries, N. Shamsaei. Fatigue behavior and modeling of additively manufactured Ti-6Al-4V including interlayer time interval effects. TMS Journal of Materials. 69(2017), 12: 2698-2705.

[17] Y. Zhai, H. Galarraga, D. A. Lados. Microstructure evolution, tensile properties, and fatigue damage mechanisms in Ti-6Al-4V alloys fabricated by two additive manufacturing techniques. Procedia Engineering. 114(2015): 658-666.

[18] O. A. Quintana, W. Tong. Effects of oxygen content on tensile and fatigue performance of Ti-6Al-4V V manufacture by selective laser melting. TMS Journal of Materials. 69(2017), 12: 2693-2697.

[19] P. Li, D. H. Warner, A. Fatemi, N. Phan. Critical assessment of the fatigue performance of additively manufactured Ti-6Al-4V and perspective for future research. International Journal of Fatigue. 85(2016): 130-143.

[20] H. Gong, K. Rafi, T. Starr, B. Stucker. Effect of defects on fatigue tests of as-built Ti-6Al-4V parts fabricated by selective laser melting. The Proceedings of the International Solid Freeform Fabrication (SFF) Symposium, Austin, TX, 2012.

[21] M. F. Ashby. The properties of foams and lattices. Philosophical Transactions of the Royal Society A. 364(2006): 15-30.

[22] L. Yang. A study about size effects of 3D periodic cellular structures. Proceedings of the 27th International Solid Freeform Fabrication (SFF) Symposium, Austin, TX, 2016.

[23] L. Yang, O. Harrysson, H. West, D. Cormier. Compressive properties of Ti-6Al-4V auxetic mesh structures made by electron beam melting. Acta Materialia. 60(2013): 3370-3379.

[24] L. Yang, O. Harrysson, H. West, D. Cormier. Mechanical properties of 3D re-entrant honeycomb auxetic structures realized via additive manufacturing. International Journal of Solids and Structures. 69-10(2015): 475-490.

[25] P. Heinel, C. Korner, R. F. Singer. Selective electron melting of cellular titanium: mechanical properties. Advanced Engineering Materials. 10(2008), 9: 882-888.

[26] J. Parthasarathy, B. Starly, S. Raman, A. Christensen. Mechanical evaluation of porous titanium (Ti6Al4V) structures with electron beam melting (EBM). Journal of the Mechanical Behavior of Biomedical Materials. 3(2010): 249-259.

[27] J. Zhou, W. O. Soboyejo. Compression-compression fatigue of open cell aluminum foams: macro-/micro-mechanics and the effects of heat treatment. Materials Science and Engineering A. 369(2004): 23-35.

[28] A.-M. Harte, N. A. Fleck, M. F. Ashby. Fatigue failure of an open cell and a closed cell aluminum alloy foam. Acta Materialia. 47(1999), 8: 2511-2524.

[29] Y. Sugimura, A. Rabiei, A. G. Evans, A. M. Harte, N. A. Fleck. Compression fatigue of a cellular Al alloy. Materials Science and Engineering A. 269(1999): 38-48.